Journal of Structural Geology 170 (2023) 104848

Contents lists available at ScienceDirect

Journal of Structural Geology

journal homepage: www.elsevier.com/locate/jsg

Fault damage zone and its effect on deep shale gas: Insights from 3D seismic interpretation in the southern Sichuan Basin, China

Shijie Ma [a,b], Lianbo Zeng [a,b,*], He Tian [c], Xuewen Shi [c], Wei Wu [c], Shaohang Yang [a,b], Liang Luo [a,b], Xiang Xu [d]

[a] State Key Laboratory of Petroleum Resources and Prospecting, China University of Petroleum (Beijing), Beijing, 102249, China
[b] College of Geosciences, China University of Petroleum (Beijing), Beijing, 102249, China
[c] Shale Gas Research Institute, PetroChina Southwest Oil and Gasfield Company, Chengdu, 610051, China
[d] Hunan Earthquake Agency, Changsha, 410004, China

ARTICLE INFO

Keywords:
Fault damage zone
Shale
Seismic variance attribute
Longmaxi formation
Shale gas preservation

ABSTRACT

Fault damage zones affect the preservation and enrichment of shale gas. Most fault damage zone studies are based on directly observed outcrops. In this study, we provide an example of fault damage zone analysis using 3D seismic data of deep shales buried more than 3500 m in the Sichuan Basin, China. The 3D seismic variance attribute and the cumulative frequency method were used to define the background value and then estimate the damage zone widths of different sizes of faults. We found that the damage zone widths range from 80 m to 1570 m, and trend to stabilize with the increase in displacements. The scattering caused by the relay zone can be interpreted as segment linkage mode and damage superposition related to subsidiary faults. The damage intensity decays following a power law with distance from the fault core, in agreement with field observations and the distribution of seismic variance. Damage zone widths display a significant asymmetry across the fault, and the hanging wall damage zone is generally wider than the footwall damage zone. We discuss the impact of the fault damage zone on shale gas preservation, which is related to the sealing of the direct caprock. It appears that the seismic variance attribute is an effective tool for subsurface characterization of fault damage zones and can help identify the location of deep unconventional energy.

1. Introduction

Shale gas is a major source of unconventional energy worldwide. The Sichuan Basin is the main area for deep shale gas exploration and development in China (Ma and Xie, 2018; Ma et al., 2021). Fault zones control the leakage and accumulation of shale gas; therefore, understanding the spatial distribution and width of damage zones is important to predict the location of deep hydrocarbons. The fault zones consist of the fault core and surrounding damage zone (Chester and Logan, 1986; Sagy et al., 2001; Katz et al., 2003; Savage and Brodsky, 2011). A fault core is a quasi-tabular shear zone comprised of gouge layers that accommodate most fault displacements. The fault core is often cemented and usually acts as a permeability barrier during the dormant period of the fault, depending on the earthquake cycle. The damage zone consists of fractured, brecciated, and pulverized rocks derived from the host rock, with complex fracture networks, which differ structurally, mechanically, seismically, and hydrologically from the undeformed host rock (Aydin, 2000; Kim et al., 2004; Childs et al., 2009; Faulkner et al., 2010; Matonti et al., 2012; Choi et al., 2016; Weng et al., 2016); for example, the permeability of the damage zone may be 2 to 3 orders of magnitude higher than that of the host rock. The fault damage zone width (W) is defined as the width of fault-related damage structures on both sides of the fault core, generally confined to a kilometer between the fault core and intact host rock (Shipton and Cowie, 2001; Berg and Skar, 2005; Rempe et al., 2013; Schueller et al., 2013; Choi et al., 2016).

Previous methods used to characterize fault damage zones are generally based on field and logging data that have been widely accepted, but in the petroleum industry, they lack the feasibility and appropriate resolution to characterize subsurface faults. Moreover, many investigations focus on the fault damage zones of strike-slip or normal faults, and less attention is given to reverse faults (Shipton and Cowie, 2001; Mayolle et al., 2019; Wu et al., 2019; Liao et al., 2020).

* Corresponding author. State Key Laboratory of Petroleum Resources and Prospecting, China University of Petroleum (Beijing), Beijing, 102249, China.
E-mail addresses: msj_2019@outlook.com (S. Ma), lbzeng@sina.com (L. Zeng), th1556243165@163.com (H. Tian), shixuewen@petrochina.com.cn (X. Shi), wuwei06@petrochina.com.cn (W. Wu), shyangsgsg@163.com (S. Yang), luoliang1225@163.com (L. Luo), xuxiangdike@163.com (X. Xu).

https://doi.org/10.1016/j.jsg.2023.104848
Received 15 September 2022; Received in revised form 4 March 2023; Accepted 20 March 2023
Available online 26 March 2023

The characterization of subsurface fault damage zones is challenging due to the limitation of subsurface data (Faulkner et al., 2010; Busetti et al., 2012; Ellis et al., 2012). Seismic attribute analysis provides an indirect method for detecting subsurface fault zones (Iacopini and Butler, 2011). Seismic attributes are used to visually enhance structures of interest in seismic images, such as azimuth, dip angle, coherence, and variance, which have been used to characterize the structure of fault zones (Chopra and Marfurt, 2007; Botter et al., 2016; Liao et al., 2017; Zhang et al., 2022). Although fractures are invisible at the seismic scale, because of the limitation of the seismic resolution, their cumulative effects can be detected as the distortion of the signal (Chopra and Marfurt, 2007). Numerical simulations of fault models and related seismic responses show the potential to characterize the size and geometry of fault damage zones using seismic attributes and seismic tomography (Botter et al., 2016, 2017). It has been demonstrated that the seismic variance attribute reflects the intensity of structural discontinuities and provides the feasibility of quantitatively evaluating the fault damage zone width (Liao et al., 2019, 2020).

The present research uses the 3D seismic variance attribute to image the subsurface reverse fault system in the southern Sichuan Basin, investigates the width and asymmetry of the fault damage zones by using scanning lines and the cumulative frequency method, and then analyses the scaling of fault displacement (D) and fault damage zone width (W). We discuss the implications of the results and investigate the relationship between the damage zone and the shale gas reservoirs.

2. Geological settings

2.1. Tectonic backgrounds

The Sichuan Basin, located in southwest China (Fig. 1a), is a superimposed basin developed in the Upper Yangtze platform and an important shale gas production area in China (Ma et al., 2020), which has undergone multi-stage subsidence, uplift, and exhumation since the Proterozoic. The Sichuan basin is dominated by three stages of basin evolution: (a) a marine carbonate platform from the Ediacaran to Middle Triassic, (b) a foreland basin with fold deformation from the Late Triassic to Late Cretaceous, and (c) subsequent exhumation uplift and structural adjustment from the late Cretaceous to the Quaternary (Deng et al., 2013; Liu et al., 2021).

Our focus is located in the southern gentle structural zone (Fig. 1a), which is bounded by the Qiyue fault belt in the east, Huaying fault belt in the west. Narrow anticlines and wide synclines developed in the study area (Fig. 1b). The deformation propagated from the Yangtze block into the eastern Sichuan Basin with a boundary at the Qiyue thrust, and the structural deformation is characterized by a thin-skinned fold-and-thrust belt (Fig. 1c). The stratigraphic succession is composed of competent layers separated by three main detachment layers (Gu et al., 2021). The

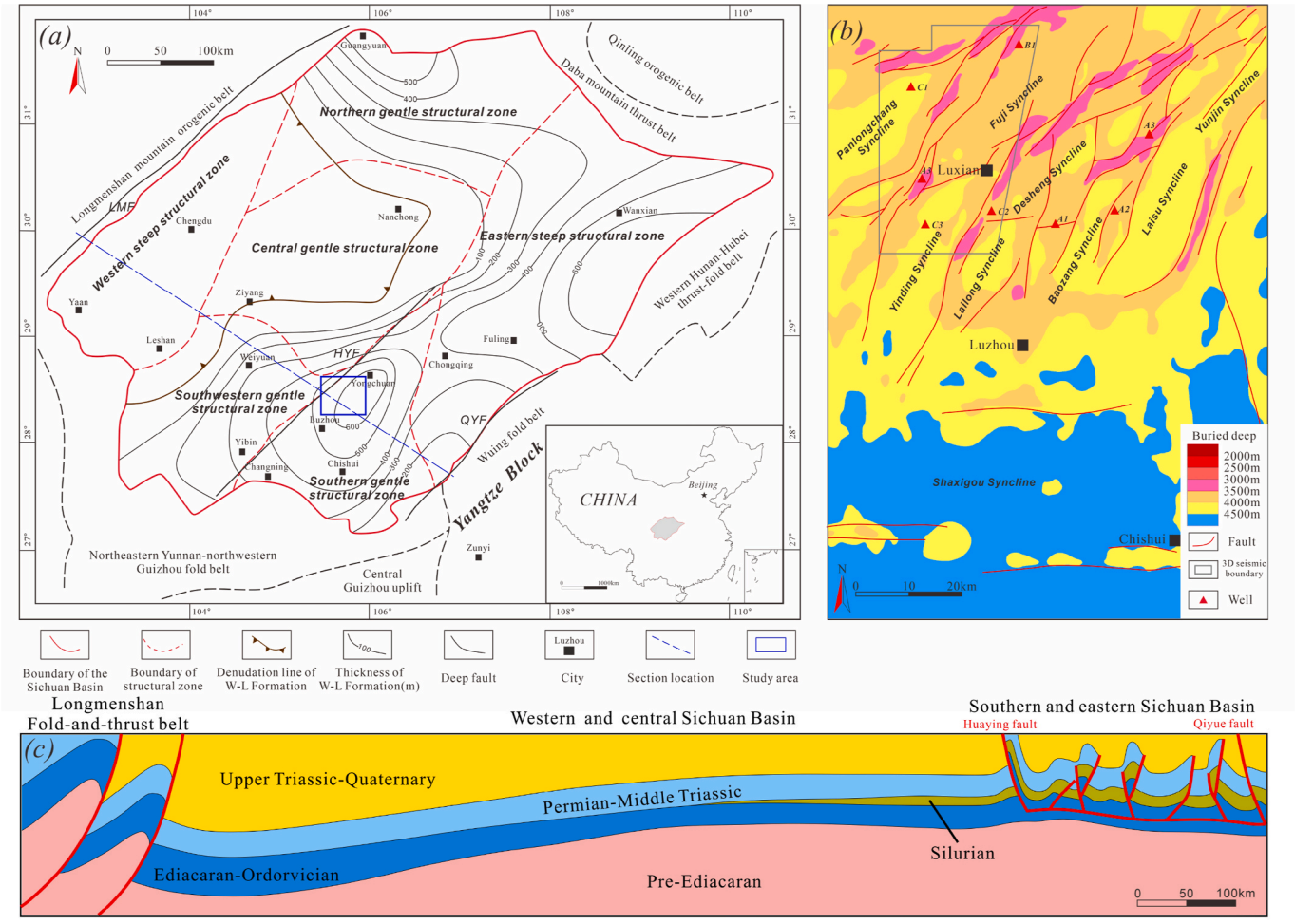

Fig. 1. (a) Location of the study area (the blue rectangle) and tectonic units of the Sichuan Basin modified from (Dai et al., 2014). (b) Structural features in the Southern Sichuan Basin, China. The red solid lines indicate the faults, and different colors indicate different burial depths, showing the form of a wide gentle syncline and narrow steep anticline, and the red triangles are wells. (c) Simplified cross section across the Sichuan Basin from NW to SE, including the Longmenshan mountain orogenic belt in the NW, the western and central Sichuan Basin, and the Southeast Sichuan which is bounded by Huaying fault and Qiyue fault. (For interpretation of the references to color in this figure legend, the reader is referred to the Web version of this article.)

basal Cambrian evaporites controlled the formation and development of the thin-skinned fold-and-thrust belt. The middle (Silurian shales) and top (Triassic evaporites) detachments accommodate displacement during the deformation.

Since the Paleozoic, the southern Sichuan Basin has undergone several tectonic movements. The remarkable structural feature is the multiple reverse fault groups (Fig. 1b) with different trends and their superposition (Li et al., 2020). The Longmaxi Formation in the study area was affected by the Yanshanian to Himalayan Orogeny, expressed by three phases of deformation from Late Cretaceous to Oligocene. The first one is characterized by the most developed NE-SW reverse faults. A second S–N-oriented compression is marked by E-W reverse faults. A last nearly E-W compressional stage is visible with nearly S–N reverse faults.

2.2. Stratigraphic units

The Longmaxi Formation was deposited in the Early Silurian after the Ordovician glacial period, which is the main gas-producing layer in Sichuan Basin (Ma et al., 2020) (Fig. 2). Submember 1 of the Longmaxi Formation is mainly siliceous and carbonaceous shale, containing siliceous biological fossils, with high organic carbon contents (>3%), high gas contents, and overpressure. Submember 2 of the Longmaxi Formation is mainly dark gray clay shale and black silty shale, while siliceous and organic carbon content is low. In this study, the total thickness of the targeted layer ranges from 200 m to 500 m. According to the basin modeling (Gao et al., 2019), rapid subsidence during the Triassic and Jurassic with a maximum burial during the Cretaceous was followed by significant uplift, erosion, and deformation during the Himalayan period (Ge et al., 2016; Li et al., 2020). The main phase of hydrocarbon generation began in the Triassic, before the maximum burial at the Late Cretaceous, and peaked during the Early Cretaceous (Shangbin et al., 2017). During the late Yanshanian (Late Cretaceous), the depth to the bottom of the Longmaxi Formation was more than 7000 m and the black shale was highly matured (Ro>2.8%) (Liu et al., 2016). At present, the burial depths of the Longmaxi Formation mainly range from 2500 m to 4500 m. In general, the burial history of the target layer is characterized by early subsidence and late uplifting. The formation of reverse fault groups with different scales and directions affected the preservation of shale gas, from Yanshanian to Himalayan.

3. Materials and methods

3.1. Methodology of seismic attributes

Detailed interpretation of seismic attributes along seismic profiles or strata slices revealed more changes in subsurface structural characterization than observable from the seismic amplitude data alone (Sarkar et al., 2010). In this study, we used a set of high-resolution 3D seismic reflection data collected in 2018, which contains abundant fault information. It was processed via poststack time migration with a dominant frequency of 25 Hz. The seismic data, which cover an area of 1000 km^2, were recorded in two-way time ranging from 500 ms to 4000 ms and converted to depth. The average error of time-to-depth conversion is less than 0.3%. The seismic and formation data were from the Shale Gas Research Institute, Southwest Oil and Gas Field Company, PetroChina. Seismic attribute extraction and seismic tomography were performed with Petrel.

We computed the volumetric seismic variance attribute, which integrated the cumulative seismic effects caused by deformation (e.g., faults and fractures) (Chopra and Marfurt, 2007; Iacopini and Butler,

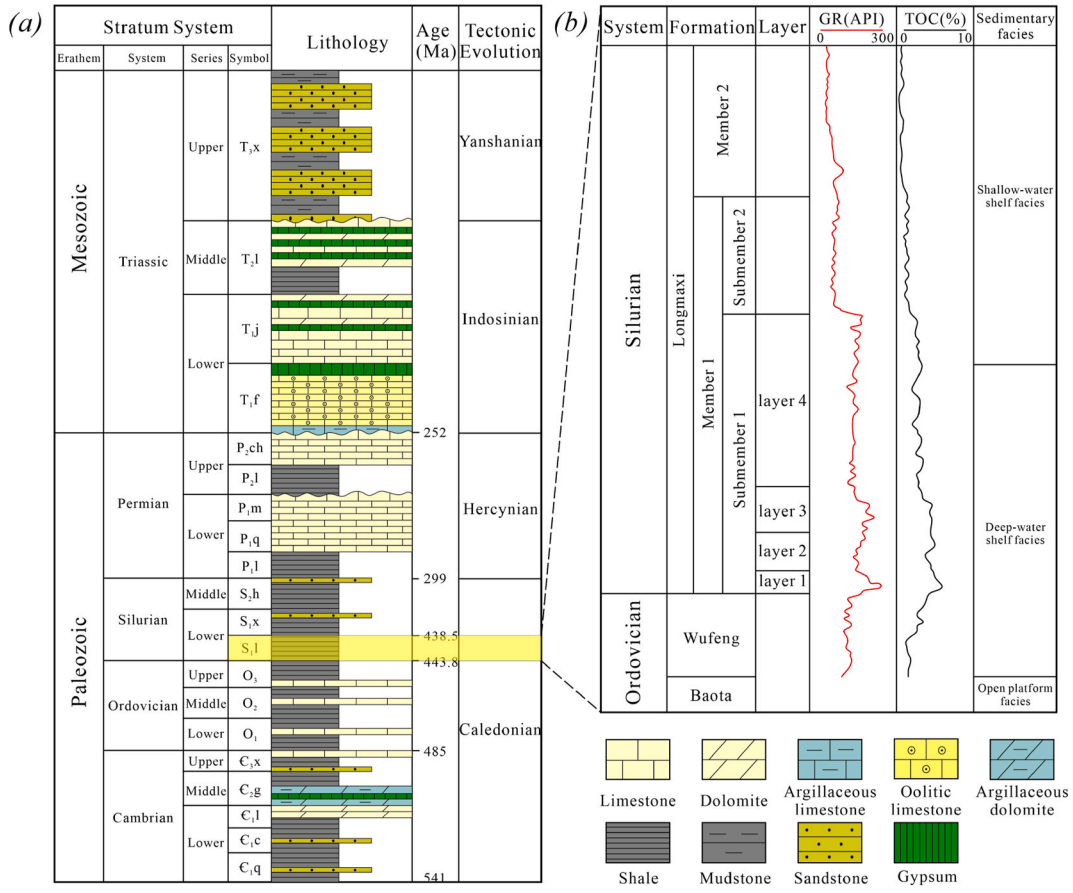

Fig. 2. The stratigraphic column in the southern Sichuan Basin including the lithological combination (a). The enlarged part marked by the yellow rectangle (b) represents the targeted strata in this study. (For interpretation of the references to color in this figure legend, the reader is referred to the Web version of this article.)

2011; Liao et al., 2019).

It is defined as

$$S^2 = \frac{1}{n}\sum_i^n (x_i - \bar{x})^2 \quad S^2(x_i) = \frac{S_i - S_{min}}{S_{max} - S_{min}}$$

where x_i indicates the energy value of a sample point, $\bar{x}$ indicates the average energy value of the sample points, and n indicates the number of samples. The seismic variance values in this study are normalized.

Variance is a measurement of the discontinuity of seismic reflectors, which has been widely used to visualize faults (Chopra and Marfurt, 2005; Zhang et al., 2022) and to estimate the damage zone widths and evaluate structural characteristics (Liao et al., 2019) and has been verified to have good similarity with the observation results of the field (Mitchell and Faulkner, 2009; Savage and Brodsky, 2011). The trace-to-trace amplitude variation could be detected by the variance attribute, which represents the trace-to-trace variability. Similar traces show low variance coefficients, while discontinuities produce high variance coefficients (e.g., fractures/faults). In the present study, the variance value is analogous to the fracture density. The zone with increased variance near the fault was regarded as the fault damage zone. The normalized variance value ranged from 0 to 1; the larger the variance value was, the higher the intensity of the structural discontinuity. The area of highest variance was interpreted as the fault core, the area of intermediate variance was interpreted as the damage zone, and the area of low variance was interpreted as the host rock far from the fault (Fig. 3).

3.2. Methodology of fault displacement

Seismic interpretation is a key method to identify subsurface fault zones. Faults can be identified by discontinuities on seismic profiles, which are shown as a break in continuous reflectors. Small faults are shown as simple discontinuities of reflectors; however, large faults are shown as a belt of disturbed reflectors with a certain width on the seismic profile (Iacopini et al., 2016). In this study, we first identified the location of the faults, and then set up scanning lines on the plane to get the seismic profiles. Straight fitted-lines of reflector are projected to center point of deformation belt at the intercept heights T_{up} and T_{low}, where the vertical separation is then computed by aforementioned two-way time and the average velocity. The fault displacements were estimated by combining the vertical separations and fault dips. We show the geometric relationship of fault displacement in Fig. 4.

To collect more reliable displacement datasets, a set of rules are established to constrain the selection of seismic profiles and displacement acquisition. First, the reflectors at the bottom of the Longmaxi Formation must be strong, and the vertical separation of breakpoints should greater than the reflector widths on multiple contiguous slices. Second, the scanning lines have to be long enough that readily identifiable host rock variance values are captured. Last, the selected faults with different strikes and dimensions help to provide a wider range of data.

3.3. Estimation of the damage zone width

In general, the damage zone width is defined by the frequency distribution of the damage structure per unit length, such as fractures, deformation bands and cracks, which commonly decrease with distance from the fault core. The outer boundary of the damage zone is the point where the frequency of the damaged structure drops to the background value or minimum level (Beach et al., 1999; Agosta and Kirschner, 2003; Faulkner et al., 2006: de Joussineau and Aydin, 2007; Gudmundsson et al., 2010; Riley et al., 2010). This estimation method has been used in most studies. The lithology, diagenesis, fault depth, tectonic background, and deformation mechanism control the background values (Fossen and Hesthammer, 2000; Shipton and Cowie, 2001; Shipton et al., 2006; Riley et al., 2010; Savage and Brodsky, 2011; Torabi and Berg, 2011). Therefore, the background values used to limit the outer boundary of the damage zone are different in each measurement. The method based on cumulative frequency is adopted to reduce the scatter of measured damage zone width (Choi et al., 2016). The slope of the cumulative frequency indicates changes in the intensity of the damage structure, and the outer boundary of the damage zone is defined as the intersection of two oblique lines with different slopes. This point is the initial value when the cumulative frequency curve reaches the lowest slope, which represents the extensive fracture density of the host rock, so it is designated as the background value.

There are many methods to detect change points, including Bayesian Information Criterion (BIC) and the Optimal Partitioning method (Main et al., 1999; Lavielle, 2005; Killick et al., 2012), which have been widely used. Since our datasets are cumulative variance based on indirect data, we use the Optimal Partitioning method to detect change points that can minimize the total residual of the split data. Variance profiles from scanning lines on different fault sizes in the Longmaxi Formation were used to estimate damage zone widths. The average variance within the unit distance is shown in a bar graph, while the cumulative variance value is shown in dots. The change point can be clearly distinguished by the distribution of the variance curve, representing the outer boundary of the damage zone. A unified standard in the cumulative frequency method is helpful to reduce the scatter of datasets in the process of estimating damage zone width.

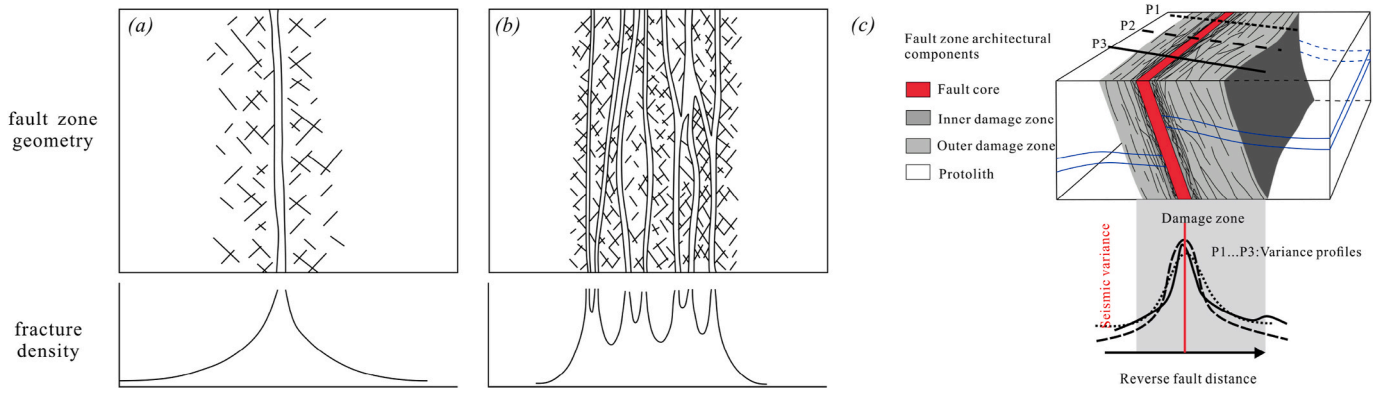

Fig. 3. Conceptual model of fault zone structure. Isolated fault cores (a) and multiple fault cores (b) are surrounded by damage zones, and the geometry and interaction of fault zones control the fracture density (Faulkner et al., 2010). (c) Schematic diagram shows the fault zone architectural components for a reverse fault modeled after (Liao et al., 2020). The Pi refers to seismic variance profiles perpendicular to fault strike. Note that red indicates fault core, gray indicates damage zones, and blank white indicates the host rock. (For interpretation of the references to color in this figure legend, the reader is referred to the Web version of this article.)

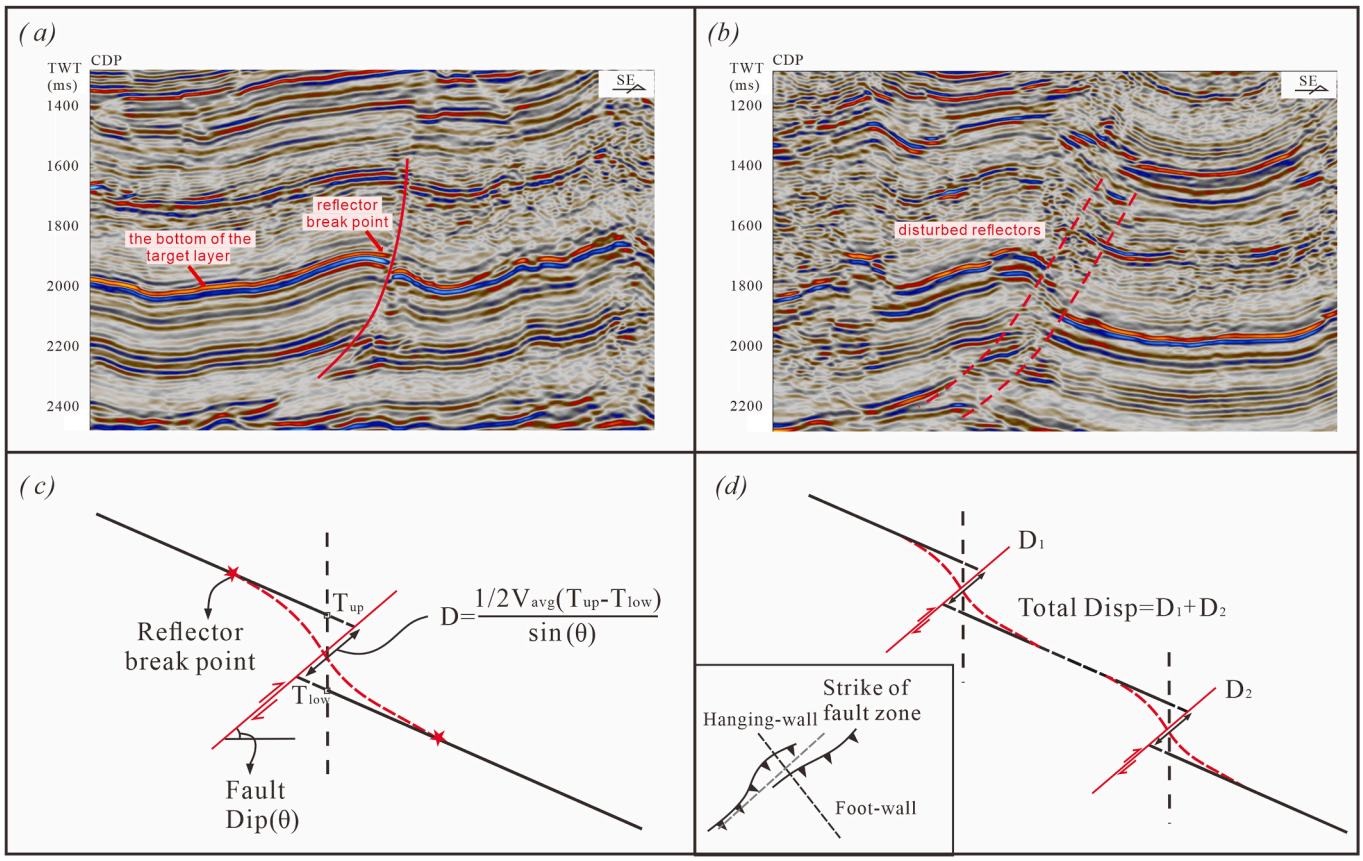

Fig. 4. Method for estimating fault displacement along the seismic profile. (a) The small fault displays a simple break of continuous reflectors. (b) The large fault displays a belt of disturbed reflectors. (c) Red lines with slip directions indicate the fault planes, and θ is fault dip. The fault displacement is calculated through difference in two-way time (TWT), average velocity and the sine of fault dip. (d) Method of fault displacement on multiple fault planes, similar to (c). (For interpretation of the references to color in this figure legend, the reader is referred to the Web version of this article.)

4. Attribute results and analysis

4.1. Fault distribution characteristics

This study focused on medium faults and large faults because of the seismic resolution, which is greater than 10 m. Faults are relatively developed from the Qiongzhusi Formation to the Feixianguan Formation. The fault dip gradually increases from the bottom to the top, ranging from 60° to 85°. Most faults disappear in the Silurian strata, and concurrently, a few faults cut through the Permian strata. We divided faults into primary faults and secondary faults, taking the top of the Longmaxi Formation or the bottom of the Xiaoheba Formation ($S1_x$) as the boundary. The primary faults cut through the Longmaxi Formation and extend upward to the internal Silurian or Permian strata (Fig. 5), which control the structural form, with displacements greater than 500 m. Some subsidiary faults are usually associated with the primary faults, which are shown as a belt of disturbed reflectors with a certain width on the seismic profile. The secondary faults do not cross the Longmaxi Formation and have displacements ranging from 20 m to 200 m. The isolated secondary faults developed at the syncline (Figs. 5 and 6), are shown as simple discontinuities of continuous reflectors on the seismic profile. Three secondary faults (F1–F3) and three primary faults (F4–F5) were investigated under the constraint of the rules (Fig. 6), and we prepared variance profiles crossing six selected faults from fault core to host rock, which revealed the variance distribution curve.

4.2. Characteristics of damage zone

The fault dip angle and displacement are measured from the seismic profiles. The fault damage zone widths are estimated by using the cumulative frequency method of the seismic variance attribute value. We focused on three characteristics of the damage zones, including the damage zone width, the asymmetry of the damage zone, and the damage decay factor.

The variance profiles (Figs. 7 and 8) reveal two groups of damage zones, and the cumulative frequency method is used to estimate the damage zone width (Fig. 9). Fig. 10 shows a plot of D versus W measured from the variance profiles.

(1) The secondary fault damage zone has a single peak in the section, and the single fault core shows the highest variance value. With increasing distance from the fault core, the variance decays rapidly to the background value. The zone with intermediate variance values is distributed on both side of the fault core, which is called the fault damage zone. The damage zone widths range from 80 to 200 m (Fig. 10). In general, the variance values of isolated secondary faults are asymmetric (Fig. 7a–c), the hanging-wall damage zone tends to be larger than the footwall damage zone (Fig. 9). The variation of damage zone along the fault is shown in Fig. 8, the isolated secondary fault has a single damage zone with no subsidiary damage structures.

(2) The primary fault damage zone has multiple variance peaks that are dominated by subsidiary faults. The damage zone widths range from 330 m to 1570 m (Fig. 10). There are strong asymmetric curves in the variance image, with multiple variance peaks on both sides of the fault core (Fig. 7d–f) and multiple slopes in the cumulative variance frequency map (Fig. 9), indicating that the primary fault includes different linked segments and multiple

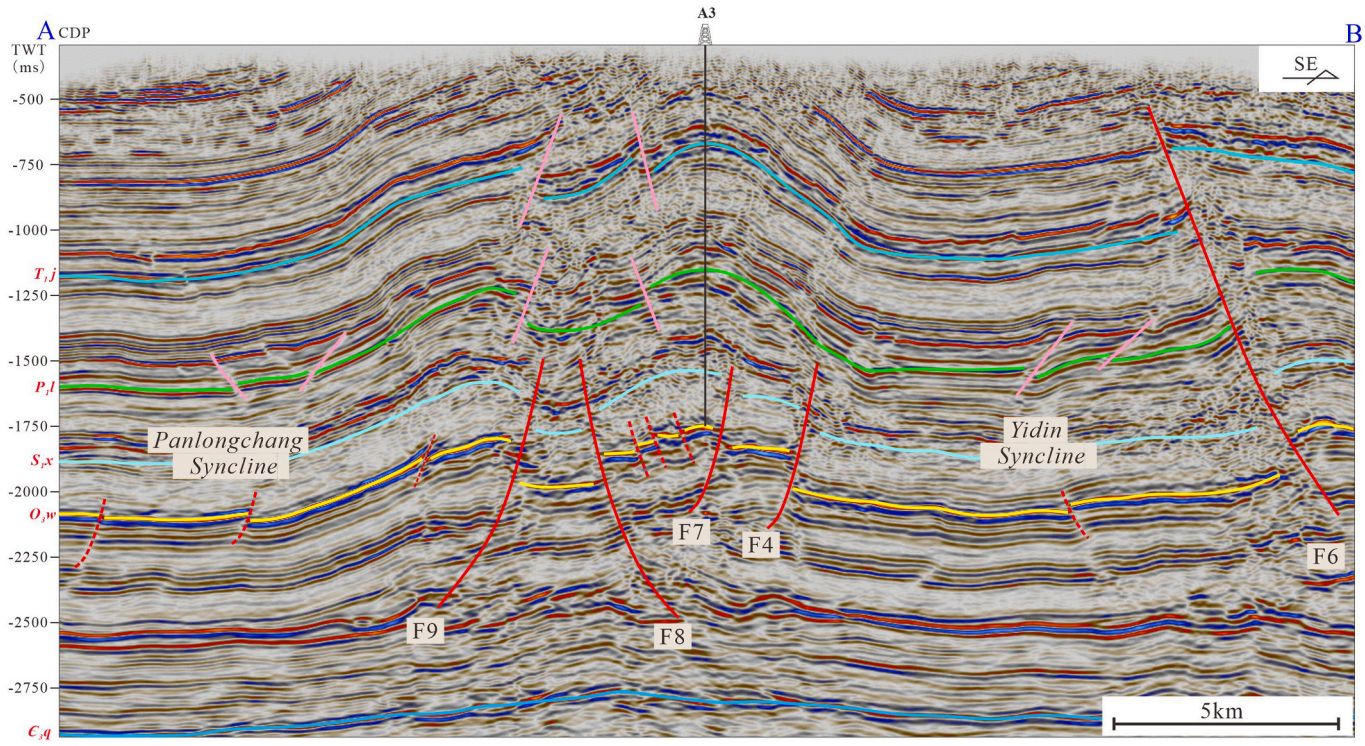

Fig. 5. Seismic response of faults on the seismic profile. The red solid line indicates the primary fault of the Longmaxi Formation, the red dotted line indicates the secondary fault of the Longmaxi Formation, and the pink dotted line indicates the fault of other strata. The horizontal axis is the common depth point (CDP), and the vertical axis is the two-way travel time (TWT). The location of this section is in Fig. 6. (For interpretation of the references to color in this figure legend, the reader is referred to the Web version of this article.)

subsidiary faults. The strong asymmetric is the consequence of damage superposition associated with multiple subsidiary faults. Variance profiles of strike intervals interval display that the primary fault has stronger geometric structure variations on the plane (Fig. 8). The damage zone in the simple geometric area of the fault presents a single master fault core, or is accompanied by a small number of subsidiary damage structures; however, there are multiple master fault cores with multiple subsidiary faults in the relay zone, which is the result of complex deformation caused by fault segments interaction. Note that the damage zones in the relay zone are wider than the simple geometries of the fault at the same displacement.

Previous field analysis has suggested that the density of the damage structure decays from the fault core to the host rock and used different methods to characterize the fracture distribution for exposed faults. There are mathematical models of off-fault distance and fracture density changes, including log-normal, gamma, power law, and exponential law (Chester et al., 2005; Faulkner et al., 2008; Savage and Brodsky, 2011), among which the power law function fit is preferred for the damage zone because the stress decays with distance following a power law trend during dynamic fault propagation (Freund, 1979). Savage and Brodsky (2011) proposed that $F=F_0r^{-n}$, where F is the fracture density, F_0 is the specific constant of the fault (the fracture density at the unit distance from the fault), r is the distance from the fault core, and n is the damage decay factor, which can also indicate the evolution stage of faults. In the present study, the fracture density is analogous to the variance value. Fig. 11 shows the seismic variance as a function of distance from the fault core for the aforementioned faults. The variance is well fit by the power law function $F=F_0r^{-n}$. The damage decay factor of the secondary fault is larger, with n ranging from 0.80 to 1.07 (average value is 0.90). However, subsidiary fault cores within the primary fault damage zone cause multiple peaks, which lead to a smaller decay factor, with n ranging from 0.29 to 0.48 (average value is 0.39). The decay factors of primary faults are from the damage zone related to the master fault that ignored the effect on subsidiary faults. Note that the primary fault decay is modeled as a composite power-law function (Fig. 11d–f), which is on the assumption that each fault (including the master fault) has a more than $r^{-0.8}$ decay in variance, as per the isolated secondary faults in our study.

5. Discussion

5.1. Scaling of damage width with displacement

The decay of variance is unambiguously related to the fault process. The decay factor n of the fault seems to decrease with the maturity of the fault (Savage and Brodsky, 2011). It can be interpreted as a result of the distribution of slip onto subsidiary faults within the damage zones. The decay factor n of the primary fault in the study area is less than 0.8, and the decay factor n of the secondary fault is greater than 0.8, indicating that the primary faults have a more mature damage zone than the secondary faults (Fig. 11). We explain this difference as the formation of subsidiary faults by fracture coalescence or fault interaction, and we model the damage distribution around primary faults as overlapping damage zones of multiple, subsidiary faults, using the damage distribution provided by the isolated faults. The field acquisition confirms the feasibility of this superposition modeling in large faults (Savage and Brodsky, 2011). Therefore, the occurrence of subsidiary structures is expected to have a broader distribution of damage, resulting in a reduction in the decay factors.

Previous studies have shown that the damage zone width (W) is proportional to the displacement (D) (Beach et al., 1999; Fossen and Hesthammer, 2000; Torabi and Berg, 2011). The damage zone width increases in equal proportion with increasing displacement (Scholz, 2002). In contrast, some investigations compiled the various fault

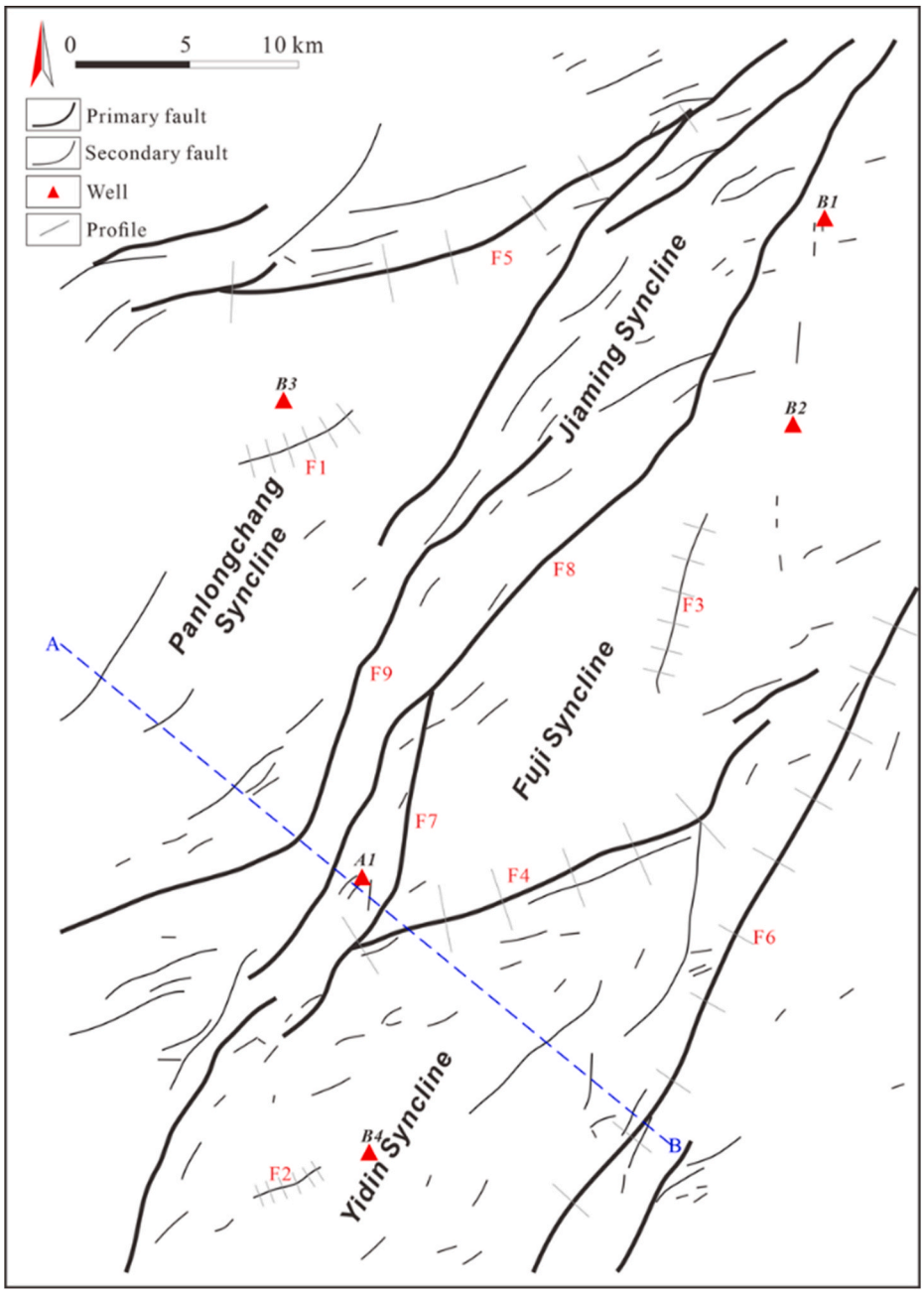

Fig. 6. The plane distribution characteristics of different sizes of faults in the Longmaxi Formation in the study area. Note that the thick line indicates the primary fault and the thin line indicates the secondary fault.

damage zone widths and found that the relationship between the damage zone width and displacement is nonlinear, in which the W/D ratio varies according to the fault size (Torabi and Berg, 2011), and the rate of increase in the damage zone width slows when the displacement exceeds 2400 m (Savage and Brodsky, 2011).

Although sufficient evidence shows the positive correlation trend of the D-W relationship, their datasets display scattering of at least two orders of magnitude for a certain value of displacement (Fig. 12). The scattering of the width is the consequence of the variation vary along strike because of fault-related diagenesis, mechanical layering, segmentation (Laubach et al., 2014; Mayolle et al., 2019, 2021).

In Fig. 10, the larger scattering occurs in the primary fault damage. The damage zone widths of the relay zone grow nearly linearly, while the damage zone width of simple geometries (i.e., no intersections, no branching) tends to saturate with increasing displacement. Damage zone scaling relationships for simple geometries of faults display a least square coefficient of $R^2 = 0.97$ with an exponent $\alpha = 0.77$. The maximum damage zone width corresponds to the relay zone, which is influenced by the interaction of the subsidiary fault segments, resulting in the scattering distribution in the D-W relationship, as well as the appearance of multiple peaks and slope changes in the variance profiles. Although similar fault depths, lithologies, and the aforementioned measuring methods contribute to reducing scatter, there are obviously two groups of datasets in primary faults.

Many concepts and models have been proposed to explain the scaling of fault damage zone width, including the fault propagation process, fault displacement accumulation and fault segment linkage (Shipton and Cowie, 2001; Walsh et al., 2002; Manighetti et al., 2004; Micarelli et al., 2006; Faulkner et al., 2011; Torabi and Berg, 2011; Liu et al., 2017). Segment linkage is an important process of fault evolution that affects

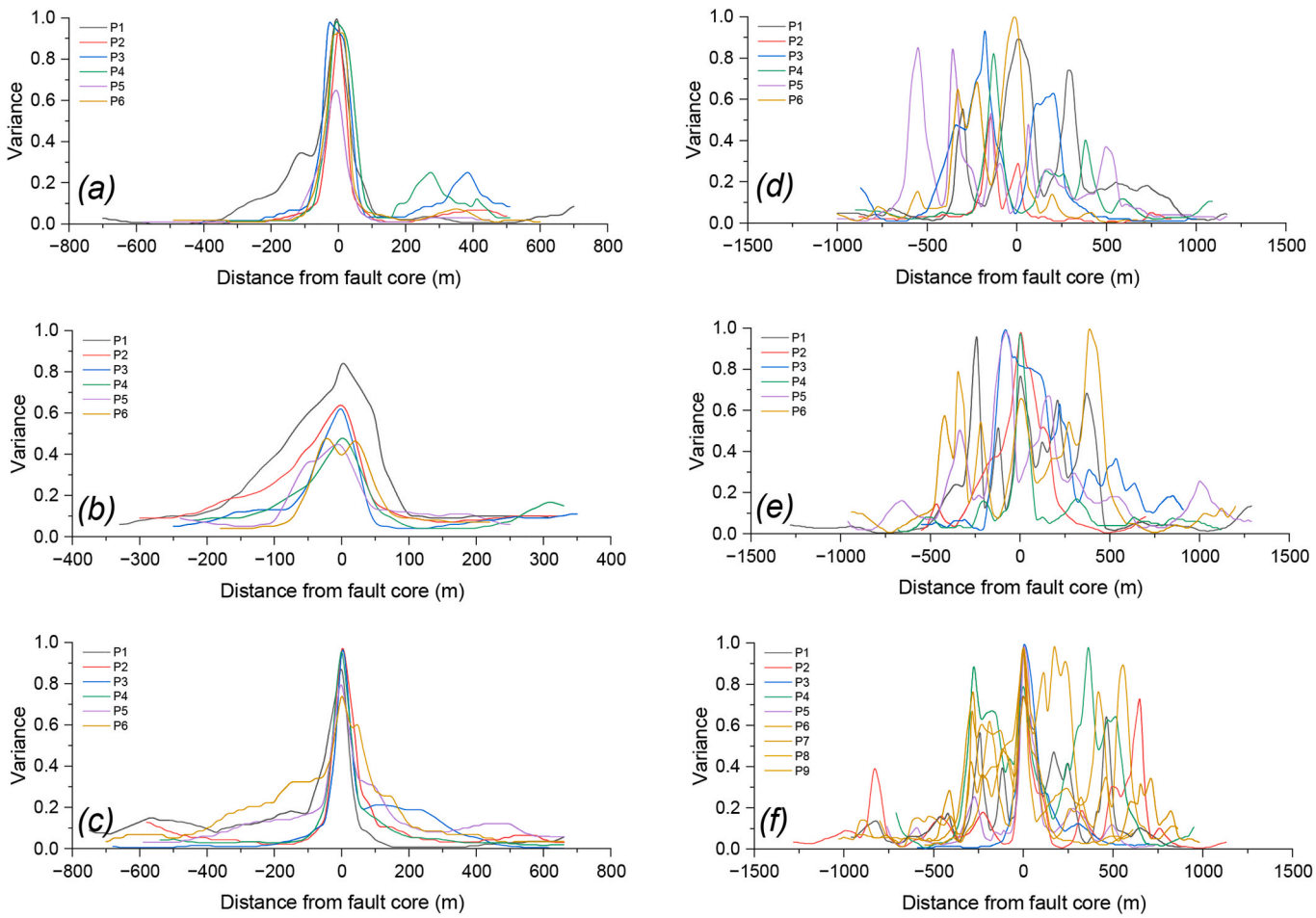

Fig. 7. Profiles of the variance values across the shale faults in the southern Sichuan Basin. A, B and C display the distribution of variance values in each scanning line perpendicular to the secondary faults, corresponding to F1, F2 and F3. C, D and E display the distribution of variance values in each scanning line perpendicular to the primary faults, corresponding to F4, F5 and F6.

the decay of the fault damage intensity and the scaling of the damage zone width (Torabi and Berg, 2011). Large faults are composed of interconnected fault segments. Field analysis shows that the growth of the reverse fault also follows the segment linkage model and that it incrementally grows through the connection of a single segment (Davis et al., 2005; Wei et al., 2020). Once all fault segments are completely connected, they will become a single fault in which displacements are evenly distributed among multiple segment. To offset the lack of displacement in relay zone, the damage growth rate of simple geometric segment with higher displacements become slow, resulting in distribution of slip onto subsidiary faults and the superposition of the damage around the relay zone.

Several solutions might be envisaged to explain the scattering of primary fault damage zone widths. The first solution is on the basis that elevated damage mainly results from subsidiary damage superposition and segment linkage events. The fault damage defined by Mode I structures is limited and might scale very differently to fault damage derived from subsidiary faults (Mayolle et al., 2019). The Mode I fracture damage zone decrease in width towards the tip of the master fault segment as displacement decreases to zero, while the subsidiary fault damage zone increases towards the master fault segment tip. In this study, the isolated secondary fault damage is mainly composed of Mode I fractures with no subsidiary faults. Contrarily, there are more subsidiary structures within primary fault damage, especially in the relay zone rather than simple geometries, and the elevated damage zone width of the relay zone can be interpreted as a result of the distribution of slip onto subsidiary faults and the superposition of the damage (Fig. 10). The bending of the D-W relationship can be interpreted as the basis that large displacement segment (e. g. simple geometries of fault segments) might have a deeper fault tip reaching the brittle-ductile transition (Nicol et al., 1996; Manighetti et al., 2001), and will not be able to link with new fault segments down dip. This change of rock mechanical behavior prevents the fault linkage and the superposition of fault damage from former faults segments.

5.2. Asymmetry of damage zone

Many investigations have shown that the damage zone width is asymmetric across the normal fault, and the hanging wall damage zone width can be larger than the footwall damage zone width (Hesthammer and Fossen, 1998; Berg and Skar, 2005; Nabavi et al., 2020). The footwall damage zone is sometimes wider than the hanging wall damage zone, and this trend is affected by the proportion of brittle rocks in both walls and the uplift of gypsum rocks (Lao et al., 2021). Lithology, fault depth, and fault geometry are all important factors controlling the asymmetry of the damage zone.

In this study, the hanging wall damage zone width of the reverse fault was larger than that of the footwall. To reduce the scatter of the subsidiary faults around the primary faults, the proportions of the width of the hanging wall and footwall damage zones of isolated secondary faults (F1, F2, and F3) are summarized, which shows that the width ratio ranges from 0.875 to 2.4 (average of 1.56), and that the fault displacements have no significant relationship with the asymmetry of the damage zone (Fig. 13).

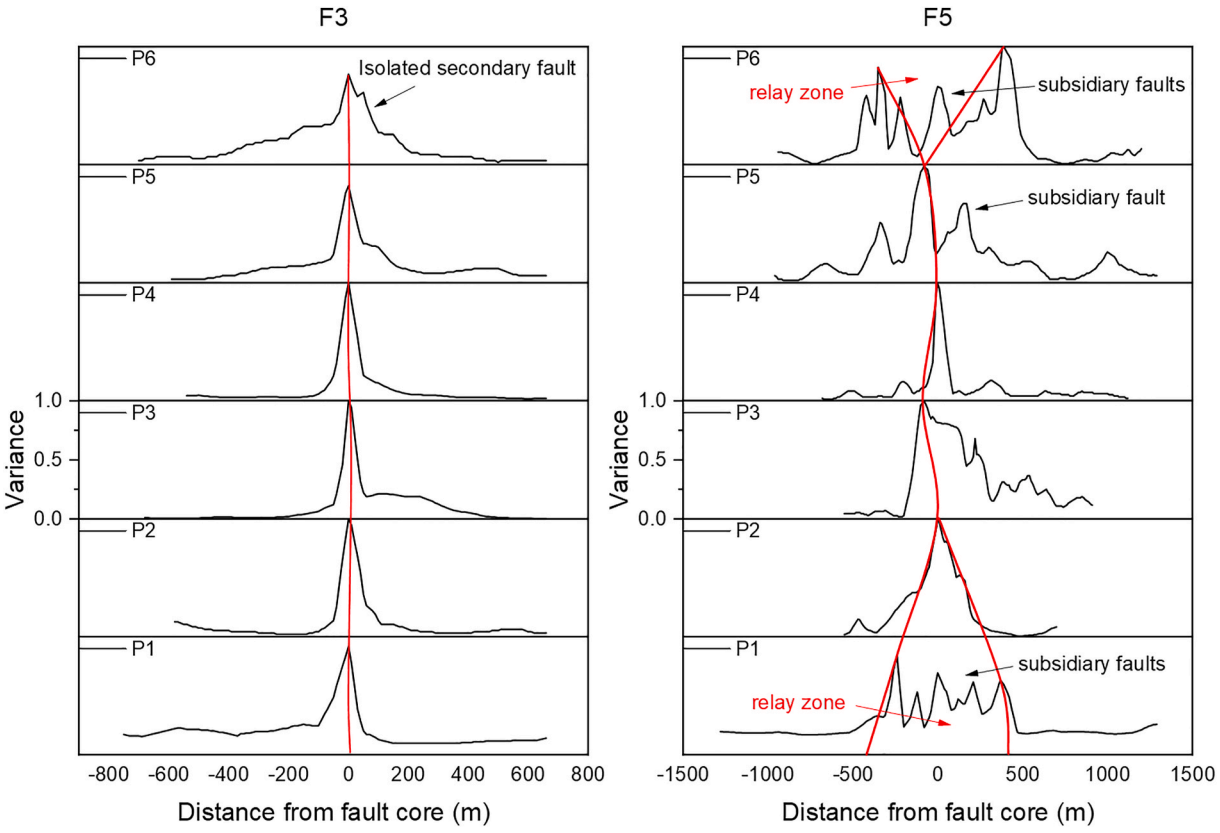

Fig. 8. Variance variations of damage zones along with strike intervals. (a) An isolated secondary fault (F3) with no subsidiary structure. (b) A primary fault (F5) with multiple primary and subsidiary fault cores in the relay zone (Profiles 1 and 6), and minor subsidiary faults in fault segments with simple geometries (Profiles 2–5). Note that the variance value between the peaks is higher than the background values, which indicates the superposition effect of the subsidiary faults.

The damaged structure is largely affected by the fold curvature of the fault propagation process when the burial depth and lithology are similar. The increase in fold curvature represents a stronger deformation (Schueller et al., 2013). In the process of fault propagation, the hanging wall is the main movable wall, and the fold curvature of the hanging wall is much higher than that of the footwall; therefore, the hanging wall damage zone contains more fractures. These accumulated discontinuities are comprehensively reflected by the variance attribute.

5.3. *Effect of damage zone on shale gas preservation*

The enrichment of hydrocarbons in organic-rich shale is essentially the result of low migration efficiency after primary hydrocarbon generation or the in situ preservation of hydrocarbons in source rocks (Jarvie et al., 2007). The quality of shale gas preservation conditions is essentially the quality of the direct caprock sealing (Jin et al., 2018; Tian et al., 2022; Xi et al., 2022). Faults are a key factor affecting the preservation of shale gas (Zeng et al., 2016). Although the fault core is usually cemented and considered to be a seepage barrier in the dormant period, the permeability of the damage zone has been widely confirmed to be 2 or 3 orders of magnitude larger than that of the host rock (Guo and Zhang, 2014), which significantly reduces the sealing property of the caprock. Apart from the seepage property of the fault, the formation time of the fault determines its influence. Large faults developed after the peak of hydrocarbon generation may promote the leakage of shale gas and destroy existing shale gas reservoirs.

The formation time of faults in the Longmaxi Formation in the southern Sichuan Basin was during the Yanshanian-Himalayan orogeny (Liu et al., 2021). The initial gas generation time of the Longmaxi Formation is Early Jurassic and the main gas generation period is in the Late Cretaceous (Liu et al., 2012). The fault formation time is mostly in the gas generation period of the highly mature and overmatured stages of shale. Therefore, the fracture network in the damage zone significantly controls the leakage and accumulation of shale gas. Production data show that all high-yield wells are located far from the primary fault damage zone (Fig. 14). Notably, well production in the primary damage zone (PDZ) is less than 10×10^4 m^3/d, and that in the secondary damage zone (SDZ) and outside of the damage zone (ODZ) is more than 20×10^4 m^3. Although the production is affected by various geological factors, the significant contrast of the production results indicates that damage zones at different scales have different effects on the preservation of shale gas.

Member 2 and submember 2 are almost gas-free (Fig. 2b) and are considered the direct caprocks of submember 1 with a high gas content (Jin et al., 2018). The primary faults cut through the whole Longmaxi Formation upward and weakened the sealing of the direct caprock because it provides a seepage channel for the leakage of shale gas. However, the secondary faults do not cross the Longmaxi Formation or only cut through submember 1. The open fractures in the secondary damage zone provide porosity to shale reservoirs, and even completely sealed fractures are prone to reactivation (Gale et al., 2014), which has no impact on the sealing of the direct caprock and contributes to increasing production.

In general, fault size and distribution in the Longmaxi Formation are interpreted by using 3D seismic reflection data. The scaling of the D-W relationship helps evaluate the boundary of the shale gas reservoir, which contributes to the exploration of deep shale gas.

6. Conclusions

Seismic interpretation was carried out for a reverse fault system in deep shale buried more than 3500 m in the southern Sichuan Basin. The

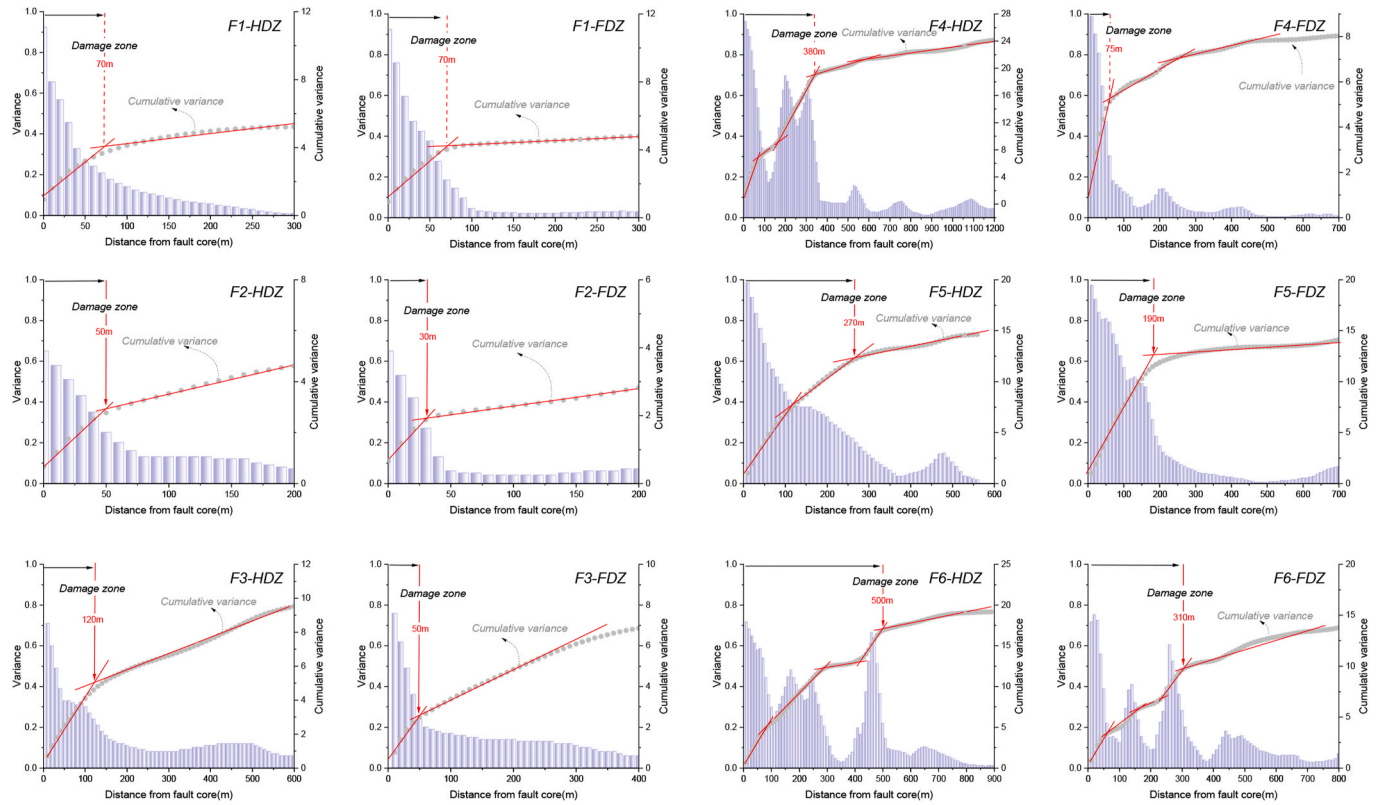

Fig. 9. The cumulative frequency method is used to estimate the damage zone width. Note that the cumulative variance diagram of the maximum displacement scanline in the six faults is displayed. HDZ is the hanging wall damage zone, and FDZ is the footwall damage zone.

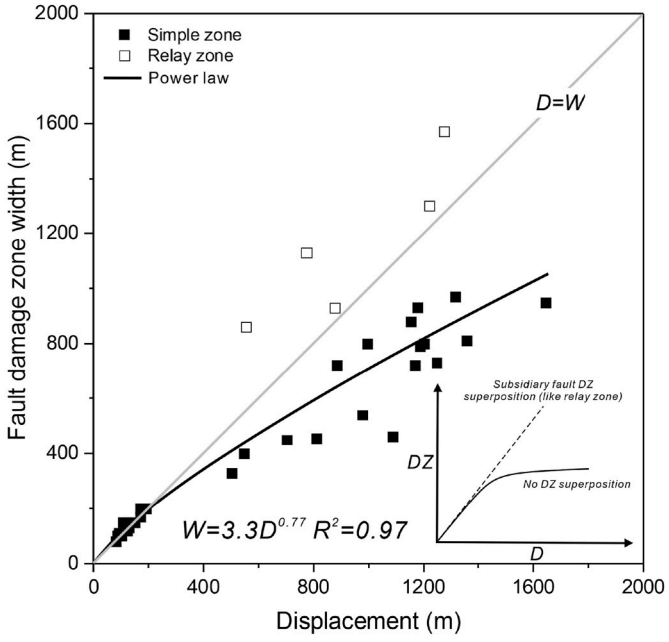

Fig. 10. D versus W measured by variance profiles. The black rectangle represents the width measured by the simple geometries (i.e., no intersections, no branching) of fault, and the hollow rectangle represents the relay zone damage width.

fault displacements and damage zone widths were estimated by variance profiles, and the damage zone widths ranged from 80 m to 1570 m. We constructed datasets of medium and large reverse faults in the shale, which suggest the following conclusions:

1. A quantitative evaluation method for damage zone width is proposed based on 3D seismic reflection data and geophysical methods. The damage zone width can be quantitatively evaluated by using the cumulative frequency method through variance profiles.
2. The variance attribute value decreases as a power law function with increasing distance from the isolated secondary fault, and the decay factors range from 0.7 to 1.03; The primary fault damage zone contains the subsidiary faults that are modeled as a composite power law with decay factors ranging from 0.29 to 0.48.
3. With increasing displacement, the damage zone width of simple geometries of faults tends to saturate (power law with an exponent of 0.77 and the constant parameter of 3.3, with a least square coefficient $R^2 = 0.97$). However, the relay damage zone width increases significantly due to the distribution of slip onto subsidiary faults and the superposition of the damage. The hanging wall damage zone width of the reverse fault is larger than that of the footwall, and the average ratio of the hanging wall and footwall damage zone widths is 1.56.
4. Different fault sizes have different effects on shale gas preservation. The primary fault weakens the sealing of the direct caprock, and the complex superimposed system of the damage zone will cause the leakage of shale gas, so drilling needs to avoid the primary damage zone. However, the secondary fault does not cut through the direct caprock, so it has no impact on the sealing of the direct caprock and shale gas preservation.

Author statemen

Shijie Ma (First author): Conceptualization, Software, Data curation, Methodology, Investigation, Formal Analysis, Validation, Visualization Writing - Original Draft; **Lianbo Zeng** (Corresponding author): Funding Acquisition, Conceptualization, Methodology, Supervision, Writing - Review & Editing; **He Tian**: Data curation, Methodology, Project

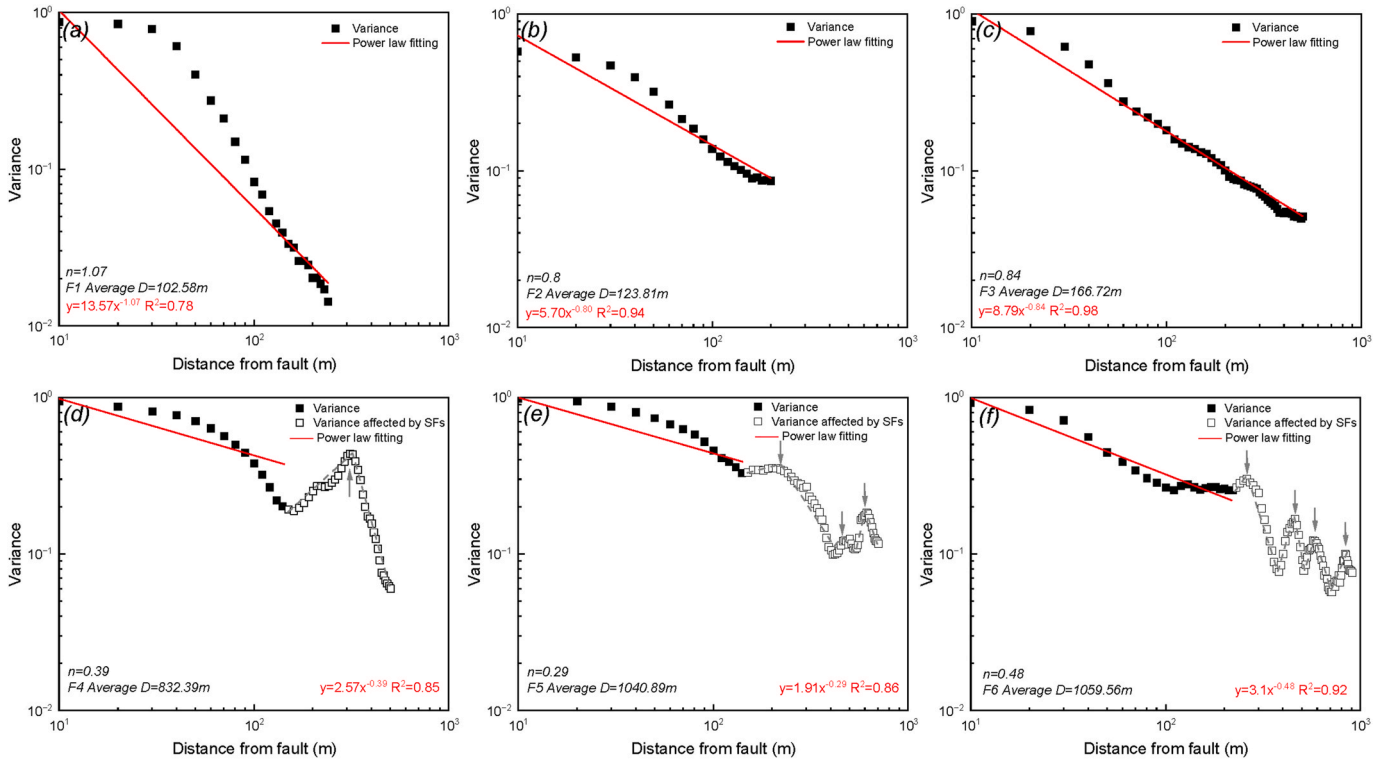

Fig. 11. The damage decay factor of the power law fits as a function of distance from fault (m). (a–c) display the power law fitting curve of secondary faults. (d–f) display the power law fitting curve of primary faults. Data points where the subsidiary faults appear to have a clear effect on the variance are ignored for the power law of best fit (represented as the points with a hollow rectangle). The gray arrow represents the subsidiary fault core. The gray dotted lines represent composite power law fitting.

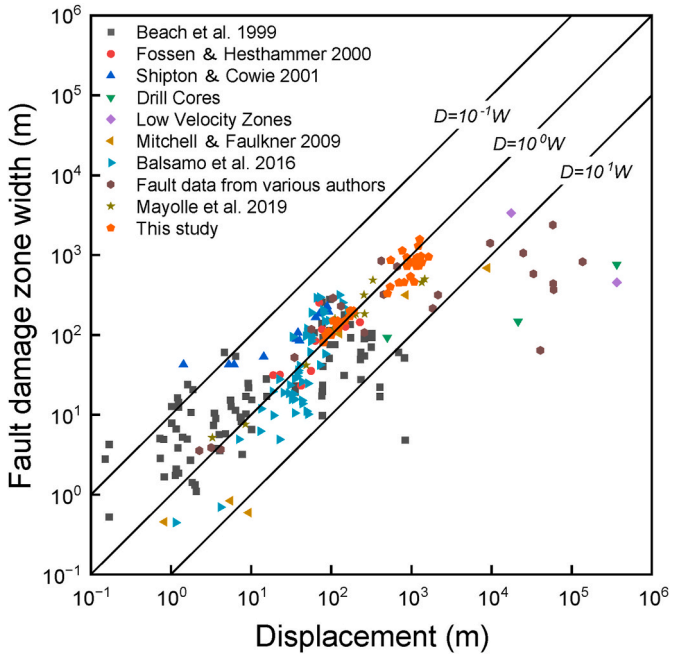

Fig. 12. Fault displacement versus damage zone width (D-W scaling relationship) for shale. Fault damage zone as a function of displacement modified from (Savage and Brodsky, 2011) and (Mayolle et al., 2019), the dataset of this study is orange. (For interpretation of the references to color in this figure legend, the reader is referred to the Web version of this article.)

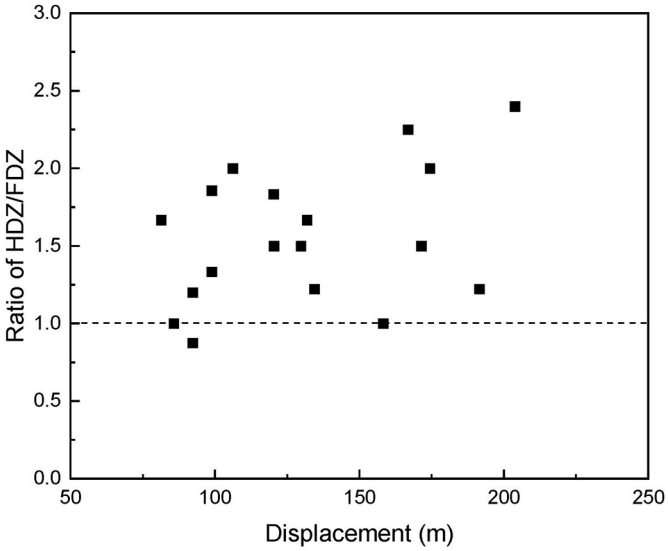

Fig. 13. Ratio of damage zone width in hanging wall and footwall. HFZ is hanging wall damage zone, and FDZ is footwall damage zone.

Administration; **Xuewen Shi**: Funding Acquisition, Supervision, Project Administration; **Wei Wu**: Funding Acquisition, Supervision, Project Administration; **Shaohang Yang**: Software, Resources, Visualization; **Liang Luo**: Software, Investigation; **Xiang Xu**: Software, Resources.

Declaration of competing interest

The authors declare that they have no known competing financial interests or personal relationships that could have appeared to influence

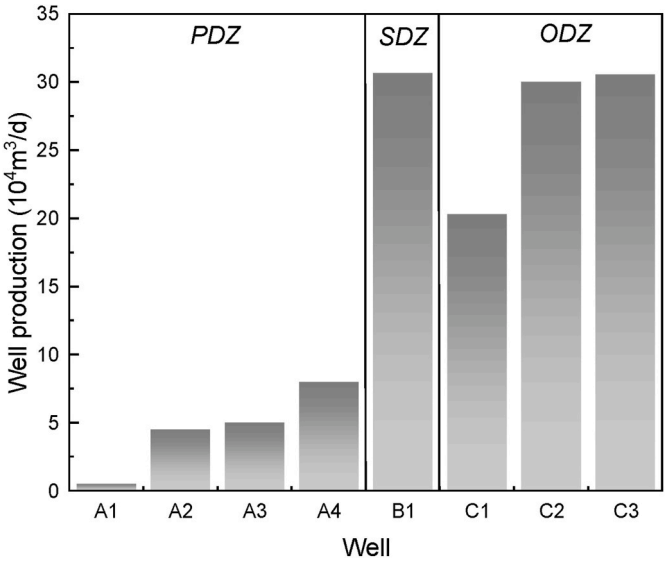

Fig. 14. The relationship between production and fault damage zone. PDZ represents the primary fault damage zone, SDZ represents the secondary fault damage zone, and ODZ represents the outside of the damage zone. Note that the production refers to the daily output of 1500m fracturing length in a well, and the data is provided by PetroChina Southwest Oil & Gasfield Company. The well location is in Fig. 1.

the work reported in this paper.

Data availability

Data will be made available on request.

Acknowledgements

This work was supported by the National Natural Science Foundation of China (Grant No. U1663203). The authors would like to thank John Hooker and three anonymous reviewers for their positive remarks and improvements.

References

Agosta, F., Kirschner, D.L., 2003. Fluid conduits in carbonate-hosted seismogenic normal faults of central Italy. J. Geophys. Res. Solid Earth 108. https://doi.org/10.1029/2002JB002013.

Aydin, A., 2000. Fractures, faults, and hydrocarbon entrapment, migration and flow. Mar. Petrol. Geol. 17, 797–814. https://doi.org/10.1016/S0264-8172(00)00020-9.

Beach, A., Welbon, A.I., Brockbank, P.J., McCallum, J.E., 1999. Reservoir damage around faults: outcrop examples from the Suez rift. Petrol. Geosci. 5, 109–116. https://doi.org/10.1144/PETGEO.5.2.109.

Berg, S.S., Skar, T., 2005. Controls on damage zone asymmetry of a normal fault zone: outcrop analyses of a segment of the Moab fault, SE Utah. J. Struct. Geol. 27, 1803–1822. https://doi.org/10.1016/j.jsg.2005.04.012.

Botter, C., Cardozo, N., Hardy, S., Lecomte, I., Paton, G., Escalona, A., 2016. Seismic characterisation of fault damage in 3D using mechanical and seismic modelling. Mar. Petrol. Geol. 77, 973–990. https://doi.org/10.1016/J.MARPETGEO.2016.08.002.

Botter, C., Cardozo, N., Qu, D.F., Tveranger, J., Kolyukhin, D., 2017. Seismic characterization of fault facies models. Interpretation.J.Subsurf.Charact 5, SP9–SP26. https://doi.org/10.1190/INT-2016-0226.1 WE - Science Citation Index Expanded (SCI-EXPANDED.

Busetti, S., Mish, K., Hennings, P., Reches, Z., 2012. Damage and plastic deformation of reservoir rocks: Part 2. Propagation of a hydraulic fracture. AAPG Bull. 96, 1711–1732. https://doi.org/10.1306/02011211011 WE - Science Citation Index Expanded (SCI-EXPANDED.

Chester, F.M., Logan, J.M., 1986. Implications for mechanical properties of brittle faults from observations of the Punchbowl fault zone, California. Pure and Applied Geophysics PAGEOPH 124, 79–106. https://doi.org/10.1007/BF00875720.

Chester, J.S., Chester, F.M., Kronenberg, A.K., 2005. Fracture surface energy of the Punchbowl fault, San Andreas system. Nature 437, 133–136. https://doi.org/10.1038/NATURE03942.

Childs, C., Manzocchi, T., Walsh, J.J., Bonson, C.G., Nicol, A., Schöpfer, M.P.J., 2009. A geometric model of fault zone and fault rock thickness variations. J. Struct. Geol. 31, 117–127. https://doi.org/10.1016/j.jsg.2008.08.009.

Choi, J.H., Edwards, P., Ko, K., Kim, Y.S., 2016. Definition and classification of fault damage zones: a review and a new methodological approach. Earth Sci. Rev. 152, 70–87. https://doi.org/10.1016/J.EARSCIREV.2015.11.006.

Chopra, S., Marfurt, K.J., 2007. Seismic Attributes for Prospect Identification and Reservoir Characterization. https://doi.org/10.1190/1.9781560801900.

Chopra, S., Marfurt, K.J., 2005. Seismic attributes - a historical perspective. Geophysics 70. https://doi.org/10.1190/1.2098670.

Dai, J., Zou, C., Liao, S., Dong, D., Ni, Y., Huang, J., Wu, W., Gong, D., Huang, S., Hu, G., 2014. Geochemistry of the extremely high thermal maturity Longmaxi shale gas, southern Sichuan Basin. Org. Geochem. 74, 3–12. https://doi.org/10.1016/J.ORGGEOCHEM.2014.01.018.

Davis, K., Burbank, D.W., Fisher, D., Wallace, S., Nobes, D., 2005. Thrust-fault growth and segment linkage in the active Ostler fault zone, New Zealand. J. Struct. Geol. 27, 1528–1546. https://doi.org/10.1016/j.jsg.2005.04.011.

de Joussineau, G., Aydin, A., 2007. The evolution of the damage zone with fault growth in sandstone and its multiscale characteristics. J. Geophys. Res. Solid Earth 112. https://doi.org/10.1029/2006JB004711.

Deng, B., Liu, S., Liu, S., Jansa, L., Li, Z., Zhong, Y., 2013. Progressive indosinian N-S deformation of the Jiaochang structure in the Songpan-Ganzi fold-belt, western China. PLoS One 8. https://doi.org/10.1371/JOURNAL.PONE.0076732.

Ellis, M.A., Laubach, S.E., Eichhubl, P., Olson, J.E., Hargrove, P., 2012. Fracture development and diagenesis of torridon group applecross formation, near an Teallach, NW Scotland: Millennia of brittle deformation resilience? J. Geol. Soc. 169, 297–310. https://doi.org/10.1144/0016-76492011-086.

Faulkner, D.R., Jackson, C.A.L., Lunn, R.J., Schlische, R.W., Shipton, Z.K., Wibberley, C. A.J., Withjack, M.O., 2010. A review of recent developments concerning the structure, mechanics and fluid flow properties of fault zones. J. Struct. Geol. 32, 1557–1575. https://doi.org/10.1016/j.jsg.2010.06.009.

Faulkner, D.R., Mitchell, T.M., Healy, D., Heap, M.J., 2006. Slip on "weak" faults by the rotation of regional stress in the fracture damage zone. Nature 444, 922–925. https://doi.org/10.1038/NATURE05353.

Faulkner, D.R., Mitchell, T.M., Jensen, E., Cembrano, J., 2011. Scaling of fault damage zones with displacement and the implications for fault growth processes. J. Geophys. Res. Solid Earth 116. https://doi.org/10.1029/2010JB007788.

Faulkner, D.R., Mitchell, T.M., Rutter, E.H., Cembrano, J., 2008. On the Structure and Mechanical Properties of Large Strike-Slip Faults, vol. 299. Geological Society Special Publication, pp. 139–150. https://doi.org/10.1144/SP299.9.

Fossen, H., Hesthammer, J., 2000. Possible absence of small faults in the Gullfaks Field, northern North Sea: implications for downscaling of faults in some porous sandstones. J. Struct. Geol. 22, 851–863. https://doi.org/10.1016/S0191-8141(00)00013-4.

Freund, L.B., 1979. The mechanics of dynamic shear crack propagation. J. Geophys. Res. Solid Earth 84, 2199–2209. https://doi.org/10.1029/JB084IB05P02199.

Gale, J.F.W., Laubach, S.E., Olson, J.E., Eichhubl, P., Fall, A., 2014. Natural fractures in shale: a review and new observations. AAPG (Am. Assoc. Pet. Geol.) Bull. 101, 2165–2216. https://doi.org/10.1306/08121413151.

Gao, J., Zhang, J., He, S., Zhao, J., He, Z., Wo, Y., Feng, Y., Li, W., 2019. Overpressure generation and evolution in Lower Paleozoic gas shales of the Jiaoshiba region, China: implications for shale gas accumulation. Mar. Petrol. Geol. 102, 844–859. https://doi.org/10.1016/j.marpetgeo.2019.01.032.

Ge, X., Shen, C., Selby, D., Deng, D., Mei, L., 2016. Apatite fission-track and Re-Os geochronology of the xuefeng uplift, China: temporal implications for dry gas associated hydrocarbon systems. Geology 44, 491–494. https://doi.org/10.1130/G37666.1.

Gu, Z., Wang, X., Nunns, A., Zhang, B., Jiang, H., Fu, L., Zhai, X., 2021. Structural styles and evolution of a thin-skinned fold-and-thrust belt with multiple detachments in the eastern Sichuan Basin, South China. J. Struct. Geol. 142, 104191 https://doi.org/10.1016/J.JSG.2020.104191.

Gudmundsson, A., Simmenes, T.H., Larsen, B., Philipp, S.L., 2010. Effects of internal structure and local stresses on fracture propagation, deflection, and arrest in fault zones. J. Struct. Geol. 32, 1643–1655. https://doi.org/10.1016/j.jsg.2009.08.013.

Guo, T., Zhang, H., 2014. Formation and enrichment mode of Jiaoshiba shale gas field, Sichuan Basin. Petrol. Explor. Dev. 41, 31–40. https://doi.org/10.1016/S1876-3804(14)60003-3.

Hesthammer, J., Fossen, H., 1998. The use of dipmeter data to constrain the structural geology of the Gullfaks Field, northern North Sea. Mar. Petrol. Geol. 15, 549–573. https://doi.org/10.1016/S0264-8172(98)00028-2.

Iacopini, D., Butler, R.W.H., 2011. Imaging deformation in submarine thrust belts using seismic attributes. Earth Planet Sci. Lett. 302, 414–422. https://doi.org/10.1016/j.epsl.2010.12.041.

Iacopini, D., Butler, R.W.H., Purves, S., McArdle, N., De Freslon, N., 2016. Exploring the seismic expression of fault zones in 3D seismic volumes. J. Struct. Geol. 89, 54–73. https://doi.org/10.1016/j.jsg.2016.05.005.

Jarvie, D.M., Hill, R.J., Ruble, T.E., Pollastro, R.M., 2007. Unconventional shale-gas systems: the Mississippian Barnett Shale of north-central Texas as one model for thermogenic shale-gas assessment. AAPG (Am. Assoc. Pet. Geol.) Bull. 91, 475–499. https://doi.org/10.1306/12190606068.

Jin, Z., Nie, H., Liu, Q., Zhao, J., Jiang, T., 2018. Source and seal coupling mechanism for shale gas enrichment in upper ordovician Wufeng formation - Lower Silurian Longmaxi Formation in Sichuan Basin and its periphery. Mar. Petrol. Geol. 97, 78–93. https://doi.org/10.1016/J.MARPETGEO.2018.06.009.

Katz, O., Reches, Z., Baer, G., 2003. Faults and their associated host rock deformation: Part I. Structure of small faults in a quartz-syenite body, southern Israel. J. Struct.

Geol. 25, 1675–1689. https://doi.org/10.1016/S0191-8141(03)00011-7 WE - Science Citation Index Expanded (SCI-EXPANDED).
Killick, R., Fearnhead, P., Eckley, I.A., 2012. Optimal detection of changepoints with a linear computational cost. J. Am. Stat. Assoc. 107, 1590–1598. https://doi.org/10.1080/01621459.2012.737745/SUPPL_FILE/UASA_A_737745_SUP_29318271.ZIP.
Kim, Y.S., Peacock, D.C.P., Sanderson, D.J., 2004. Fault damage zones. J. Struct. Geol. 26, 503–517. https://doi.org/10.1016/j.jsg.2003.08.002.
Lao, H., Wang, Y., Meng, N., Wu, Z., 2021. Architectural characteristics and evolution sequences of different types of faults in extensional basins—evidence collected from cores in the Dongying Depression. Mar. Petrol. Geol. 132 https://doi.org/10.1016/j.marpetgeo.2021.105199.
Laubach, S.E., Eichhubl, P., Hargrove, P., Ellis, M.A., Hooker, J.N., 2014. Fault core and damage zone fracture attributes vary along strike owing to interaction of fracture growth, quartz accumulation, and differing sandstone composition. J. Struct. Geol. 68, 207–226. https://doi.org/10.1016/j.jsg.2014.08.007.
Lavielle, M., 2005. Using penalized contrasts for the change-point problem. Signal Process. 85, 1501–1510. https://doi.org/10.1016/J.SIGPRO.2005.01.012.
Li, S., Li, Y., He, Z., Chen, K., Zhou, Y., Yan, D., 2020. Differential deformation on two sides of Qiyueshan Fault along the eastern margin of Sichuan Basin, China, and its influence on shale gas preservation. Mar. Petrol. Geol. 121 https://doi.org/10.1016/J.MARPETGEO.2020.104602.
Liao, Z., Hu, L., Huang, X., Carpenter, B.M., Marfurt, K.J., Vasileva, S., Zhou, Y., 2020. Characterizing damage zones of normal faults using seismic variance in the Wangxuzhuang oilfield, China. Interpretation 8, SP53–SP60. https://doi.org/10.1190/INT-2020-0004.1.
Liao, Z., Liu, H., Carpenter, B.M., Marfurt, K.J., Reches, Z., 2019. Analysis of fault damage zones using three-dimensional seismic coherence in the Anadarko Basin, Oklahoma. AAPG (Am. Assoc. Pet. Geol.) Bull. 103, 1771–1785. https://doi.org/10.1306/1219181413417207.
Liao, Z.H., Liu, H., Jiang, Z., Marfurt, K.J., Reches, Z., 2017. Fault damage zone at subsurface: a case study using 3D seismic attributes and a clay model analog for the Anadarko Basin, Oklahoma. Interpretation.J.Subsurf. Charact 5, T143–T150. https://doi.org/10.1190/INT-2016-0033.1 WE - Science Citation Index Expanded (SCI-EXPANDED).
Liu, S., Deng, B., Li, Z., Sun, W., 2012. Architecture of basin-mountain systems and their influences on gas distribution: a case study from the Sichuan basin, South China. J. Asian Earth Sci. 47, 204–215. https://doi.org/10.1016/j.jseaes.2011.10.012.
Liu, S., Deng, B., Zhong, Y., Ran, B., Yong, Z., Sun, W., Yang, D., Jiang, L., Ye, Y., 2016. Unique geological features of burial and superimposition of the Lower Paleozoic shale gas across the Sichuan Basin and its periphery. Earth Sci. Front. 23, 11–28. https://doi.org/10.13745/J.ESF.2016.01.002.
Liu, S., Yang, Y., Deng, B., Zhong, Y., Wen, L., Sun, W., Li, Z., Jansa, L., Li, J., Song, J., Zhang, X., Peng, H., 2021. Tectonic evolution of the Sichuan Basin, southwest China. Earth Sci. Rev. https://doi.org/10.1016/j.earscirev.2020.103470.
Liu, Y., Wu, K., Wang, X., Liu, B., Guo, J., Du, Y., 2017. Architecture of buried reverse fault zone in the sedimentary basin: a case study from the Hong-Che Fault Zone of the Junggar Basin. J. Struct. Geol. 105, 1–17. https://doi.org/10.1016/J.JSG.2017.11.002.
Ma, X., Wang, H., Zhou, S., Shi, Z., Zhang, L., 2021. Deep shale gas in China: geological characteristics and development strategies. Energy Rep. 7, 1903–1914. https://doi.org/10.1016/J.EGYR.2021.03.043.
Ma, X., Xie, J., 2018. The progress and prospects of shale gas exploration and development in southern Sichuan Basin, SW China. Petrol. Explor. Dev. 45, 172–182. https://doi.org/10.1016/S1876-3804(18)30018-1.
Ma, X., Xie, J., Yong, R., Zhu, Y., 2020. Geological characteristics and high production control factors of shale gas reservoirs in Silurian Longmaxi Formation, southern Sichuan Basin, SW China. Petrol. Explor. Dev. 47, 901–915. https://doi.org/10.1016/S1876-3804(20)60105-7.
Main, I.G., Leonard, T., Papasouliotis, O., Hatton, C.G., Meredith, P.G., 1999. One slope or two? Detecting statistically significant breaks of slope in geophysical data, with application to fracture scaling relationships. Geophys. Res. Lett. 26, 2801–2804. https://doi.org/10.1029/1999GL005372.
Manighetti, I., King, G., Sammis, C.G., 2004. The role of off-fault damage in the evolution of normal faults. Earth Planet Sci. Lett. 217, 399–408. https://doi.org/10.1016/S0012-821X(03)00601-0.
Manighetti, I., King, G.C.P., Gaudemer, Y., Scholz, C.H., Doubre, C., 2001. Slip accumulation and lateral propagation of active normal faults in Afar. J. Geophys. Res. Solid Earth 106, 13667–13696. https://doi.org/10.1029/2000JB900471.
Matonti, C., Lamarche, J., Guglielmi, Y., Marié, L., 2012. Structural and petrophysical characterization of mixed conduit/seal fault zones in carbonates: example from the Castellas fault (SE France). J. Struct. Geol. 39, 103–121. https://doi.org/10.1016/j.jsg.2012.03.003.
Mayolle, S., Soliva, R., Caniven, Y., Wibberley, C., Ballas, G., Milesi, G., Dominguez, S., 2019. Scaling of fault damage zones in carbonate rocks. J. Struct. Geol. 124, 35–50. https://doi.org/10.1016/J.JSG.2019.03.007.
Mayolle, S., Soliva, R., Dominguez, S., Wibberley, C., Caniven, Y., 2021. Nonlinear fault damage zone scaling revealed through analog modeling. Geology 49, 968–972. https://doi.org/10.1130/G48760.1.
Micarelli, L., Benedicto, A., Wibberley, C.A.J., 2006. Structural evolution and permeability of normal fault zones in highly porous carbonate rocks. J. Struct. Geol. 28, 1214–1227. https://doi.org/10.1016/j.jsg.2006.03.036.
Mitchell, T.M., Faulkner, D.R., 2009. The nature and origin of off-fault damage surrounding strike-slip fault zones with a wide range of displacements: a field study from the Atacama fault system, northern Chile. J. Struct. Geol. 31, 802–816. https://doi.org/10.1016/j.jsg.2009.05.002.
Nabavi, S.T., Alavi, S.A., Wibberley, C.A.J., Jahangiri, M., 2020. Normal fault networks and their spatial relationships in Plio-Quaternary sedimentary series: a case study in the Zanjan Depression, NW Iran. J. Struct. Geol. 136, 104072 https://doi.org/10.1016/J.JSG.2020.104072.
Nicol, A., Watterson, J., Walsh, J.J., Childs, C., 1996. The shapes, major axis orientations and displacement patterns of fault surfaces. J. Struct. Geol. 18, 235–248. https://doi.org/10.1016/S0191-8141(96)80047-2.
Rempe, M., Mitchell, T., Renner, J., Nippress, S., Ben-Zion, Y., Rockwell, T., 2013. Damage and seismic velocity structure of pulverized rocks near the San Andreas Fault. J. Geophys. Res. Solid Earth 118, 2813–2831. https://doi.org/10.1002/JGRB.50184.
Riley, P.R., Goodwin, L.B., Lewis, C.J., 2010. Controls on fault damage zone width, structure, and symmetry in the Bandelier Tuff, New Mexico. J. Struct. Geol. 32, 766–780. https://doi.org/10.1016/j.jsg.2010.05.005.
Sagy, A., Reches, Z., Roman, I., 2001. Dynamic fracturing: field and experimental observations. J. Struct. Geol. 23, 1223–1239. https://doi.org/10.1016/S0191-8141(00)00190-5 WE - Science Citation Index Expanded (SCI-EXPANDED.
Sarkar, S., Marfurt, K.J., Slatt, R.M., 2010. Generation of sea-level curves from depositional pattern as seen through seismic attributes-seismic geomorphology analysis of an MTC-rich shallow sediment column, northern Gulf of Mexico. Lead. Edge 29, 1084–1091. https://doi.org/10.1190/1.3485769.
Savage, H.M., Brodsky, E.E., 2011. Collateral damage: evolution with displacement of fracture distribution and secondary fault strands in fault damage zones. J. Geophys. Res. Solid Earth 116. https://doi.org/10.1029/2010JB007665.
Scholz, C.H., 2002. The mechanics of earthquakes and faulting. The Mechanics of Earthquakes and Faulting. https://doi.org/10.1017/CBO9780511818516.
Schueller, S., Braathen, A., Fossen, H., Tveranger, J., 2013. Spatial distribution of deformation bands in damage zones of extensional faults in porous sandstones: Statistical analysis of field data. J. Struct. Geol. 52, 148–162. https://doi.org/10.1016/J.JSG.2013.03.013.
Shangbin, C., Yanming, Z., Si, C., Yufu, H., Changqing, F., Junhua, F., 2017. Hydrocarbon generation and shale gas accumulation in the Longmaxi Formation, southern Sichuan Basin, China. Mar. Petrol. Geol. 86, 248–258. https://doi.org/10.1016/j.marpetgeo.2017.05.017.
Shipton, Z.K., Cowie, P.A., 2001. Damage zone and slip-surface evolution over μm to km scales in high-porosity Navajo sandstone, Utah. J. Struct. Geol. 23, 1825–1844. https://doi.org/10.1016/S0191-8141(01)00035-9.
Shipton, Z.K., Soden, A.M., Kirkpatrick, J.D., Bright, A.M., Lunn, R.J., 2006. How thick is a fault? Fault displacement-thickness scaling revisited. Geophys. Monogr. 170, 193–198. https://doi.org/10.1029/170GM19.
Tian, H., Zeng, L., Ma, S., Li, H., Mao, Z., Peng, Y., Xu, X., Feng, D., 2022. Effects of different types of fractures on shale gas preservation in Lower Cambrian shale of northern Sichuan Basin: evidence from macro-fracture characteristics and microchemical analysis. J. Petrol. Sci. Eng. 218, 110973 https://doi.org/10.1016/J.PETROL.2022.110973.
Torabi, A., Berg, S.S., 2011. Scaling of fault attributes: a review. Mar. Petrol. Geol. 28, 1444–1460. https://doi.org/10.1016/j.marpetgeo.2011.04.003.
Walsh, J.J., Nicol, A., Childs, C., 2002. An alternative model for the growth of faults. J. Struct. Geol. 24, 1669–1675. https://doi.org/10.1016/S0191-8141(01)00165-1.
Wei, Z., He, H., Sun, W., Zhuang, Q., Liang, Z., 2020. Investigating thrust-fault growth and segment linkage using displacement distribution analysis in the active Duzhanzi thrust fault zone, Northern Tian Shan of China. J. Struct. Geol. 133, 103990 https://doi.org/10.1016/J.JSG.2020.103990.
Weng, H., Yang, H., Zhang, Z., Chen, X., 2016. Earthquake rupture extents and coseismic slips promoted by damaged fault zones. J. Geophys. Res. Solid Earth 121, 4446–4457. https://doi.org/10.1002/2015JB012713.
Wu, G., Gao, L., Zhang, Y., Ning, C., Xie, E., 2019. Fracture attributes in reservoir-scale carbonate fault damage zones and implications for damage zone width and growth in the deep subsurface. J. Struct. Geol. 118, 181–193. https://doi.org/10.1016/j.jsg.2018.10.008.
Xi, Z., Tang, S., Zhang, S., Lash, G.G., Ye, Y., 2022. Controls of marine shale gas accumulation in the eastern periphery of the Sichuan Basin, South China. Int. J. Coal Geol. 251 https://doi.org/10.1016/j.coal.2022.103939.
Zeng, L., Lyu, W., Li, J., Zhu, L., Weng, J., Yue, F., Zu, K., 2016. Natural fractures and their influence on shale gas enrichment in Sichuan Basin, China. J. Nat. Gas Sci. Eng. 30, 1–9. https://doi.org/10.1016/J.JNGSE.2015.11.048.
Zhang, L., Liao, Z., Long, K., Carpenter, B.M., Zou, H., Hao, F., 2022. Fundamental constraints of lithologically-controlled fault networks on gas migration and accumulation for fractured carbonates in the western Sichuan Basin, China. J. Petrol. Sci. Eng. 208 https://doi.org/10.1016/j.petrol.2021.109502.